Specific Targeting of Highly Conserved Residues in the HIV-1 Reverse Transcriptase Primer Grip Region. 2. Stereoselective Interaction to Overcome the Effects of Drug Resistant Mutations

Stefania Butini,[†,‡] Margherita Brindisi,[†,‡] Sandro Cosconati,[§,†] Luciana Marinelli,[§,†] Giuseppe Borrelli,[†,‡] Salvatore Sanna Coccone,[†,‡] Anna Ramunno,[†,‡] Giuseppe Campiani,[†,‡,*] Ettore Novellino,[§,†] Samantha Zanoli,[⊥,†] Alberta Samuele,[⊥,†] Gianluca Giorgi,[∥] Alberto Bergamini,[#] Michela Di Mattia,[▽] Silvana Lalli,[▽] Bruno Galletti,[▽] Sandra Gemma,[†,‡] and Giovanni Maga[⊥,†]

European Research Centre for Drug Discovery and Development (NatSynDrugs), Università di Siena, Italy, Dipartimento Farmaco Chimico Tecnologico (DFCT), Università di Siena, via Aldo Moro 2, 53100 Siena, Italy, Dipartimento di Chimica Farmaceutica e Tossicologica (DCF&T), Università di Napoli Federico II, via D. Montesano 49, 80131 Napoli, Italy, Istituto di Genetica Molecolare (IGM)—CNR, via Abbiategrasso 207, 27100 Pavia, Italy, Dipartimento di Chimica (DC), Università di Siena, via Aldo Moro 2, 53100 Siena, Italy, Dipartimento di Sanità Pubblica e Biologia Cellulare, Università degli Studi di Roma "Tor Vergata", via Tor Vergata 135, 00133 Roma, Italy, Sigma-Tau Industrie Farmaceutiche Riunite spa, Via Pontina Km 30, 400, 00040 Pomezia, Italy

Received November 4, 2008

Starting from the prototypic compound **4**, we describe new, potent, and broad-spectrum pyrrolobenzo(pyrido)oxazepinones antivirals. A biochemical and enzymological investigation was performed for defining their mechanism of inhibition at either recombinant HIV-1 RT wild type and non-nucleoside reverse transcriptase inhibitors (NNRTIs)-resistant mutants. For the novel compounds (*S*)-(+)-**5** and (*S*)-(−)-**7**, a clear-cut stereoselective mechanism of enzyme inhibition was found. Molecular modeling studies were performed for revealing the underpinnings of this behavior.

Introduction

Reverse transcriptase (RT) is a key multifunctional enzyme in the life cycle of the human immunodeficiency virus type-1 (HIV-1), the causative agent of AIDS. The enzyme shows both RNA- and DNA-dependent polymerase activities and is responsible for conversion of the single-stranded RNA retroviral genome into the double-stranded proviral DNA, which is successively integrated into the host cell chromosome.[1] RT inhibitors are classified in nucleoside inhibitors (NRTIs) and non-nucleoside inhibitors (NNRTIs). The NRTIs are chain-terminators and interact competitively with the catalytic site of the RT, whereas NNRTIs interact with an allosteric site adjacent to the catalytic site of RT. Consequently, they are highly susceptible to the development of viral resistance because mutations in RT result in the preservation of the enzymatic function while impairing inhibitor binding. NNRTIs are important components of highly active antiretroviral therapy (HAART) strategies, together with NRTIs and protease inhibitors (PI).[2] NNRTIs can be grouped into two main classes: the so-called first generation NNRTIs (e.g., nevirapine, **1**, Chart 1), which are very susceptible to single-point resistance mutations within RT, and the second generation NNRTIs (e.g., efavirenz, **2**, Chart 1). These latter are characterized by higher potency, a broader spectrum of activity against HIV-1 variants, and more favorable pharmacokinetic properties. However, a rapid development of drug-resistant strains was observed upon introduction of both first and second generation drugs in therapy. Because most NNRTIs share a common binding site (with the exception of TSAO compounds and congeners),[3] one or two mutations selected by a particular drug are able to confer cross resistance to the entire class.[4] Although NNRTIs are all considered by definition noncompetitive inhibitors of RT, recent studies[4,5] have shown a peculiar mechanism of action for some of the second generation NNRTIs. Investigation of the kinetics of efavirenz binding to RT, by determination of equilibrium dissociation constants and microscopic rates of binding and dissociation, evidenced that this ligand preferentially interacted with RT complexed with both the DNA and deossinucleotide triphosphate (dNTP) substrates. It displayed lower affinity for the binary RT:DNA complex and negligible affinity for the free enzyme. Recently, we described the development of a new class of NNRTIs[6] whose prototype was the pyrrolobenzoxazepinone (PBO) **3a** (Chart 1). For this compound, a significant antiviral efficacy was combined to a limited spectrum of activity.[7] Later on, a thorough exploitation of structure-activity relationship (SAR) trends, aimed at the discovery of more potent and broad-spectrum NNRTIs allowed us the identification of a novel class

Chart 1. Reference and Title Compounds

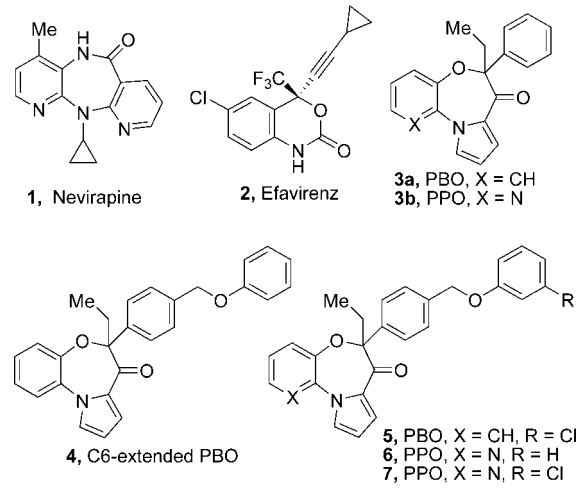

* To whom correspondence should be addressed. Phone: 0039-0577-234172. Fax: 0039-0577-234333. E-mail:campiani@unisi.it.

† European Research Centre for Drug Discovery and Development (NatSynDrugs).

‡ DFCT—Università degli Studi di Siena.

§ DCF&T—Università degli Studi di Napoli "Federico II".

∥ DC—Università degli Studi di Siena.

⊥ IGM—Istituto di Genetica Molecolare, Pavia.

DSP&BC—Università di Roma Tor Vergata.

▽ Sigma-Tau Industrie Farmaceutiche Riunite spa.

10.1021/jm801395v CCC: $40.75
Published on Web 01/26/2009

Table 1. Inhibition (*K*i, μM) of HIV-1 wt and HIV-1 Mutant RT Enzymes, Containing the Single Amino Acid Substitutions L100I, K103N, Y181I, V106A, V179D, and Y188L[a]

	K_i (μM)						
compd	wt	L100I	K103N	Y181I	V106A	V179D	Y188L
(±)-**5**	0.1 ± 0.01	0.25 ± 0.02	0.3 ± 0.02	<10	NT[b]	0.3 ± 0.02	NT[b]
(±)-**6**	0.25 ± 0.02	NT[b]	1.5 ± 0.2	<10	1.8 ± 0.2	3.6 ± 0.4	<10
(±)-**7**	0.11 ± 0.01	0.8 ± 0.1	0.8 ± 0.1	<10	NT[b]	2 ± 0.1	NT[b]
nevirapine	0.4 ± 0.03	9 ± 1	7 ± 1	36 ± 4	10 ± 1	2 ± 0.1	18 ± 2
efavirenz	0.03 ± 0.005	0.12 ± 0.01	0.16 ± 0.02	0.15 ± 0.01	0.04 ± 0.006	0.1 ± 0.01	0.38 ± 0.04

[a] All the data listed were compared to the corresponding test results for nevirapine, performed at the same time. Each value is the mean of at least three experiments ± SD. [b] NT, not tested.

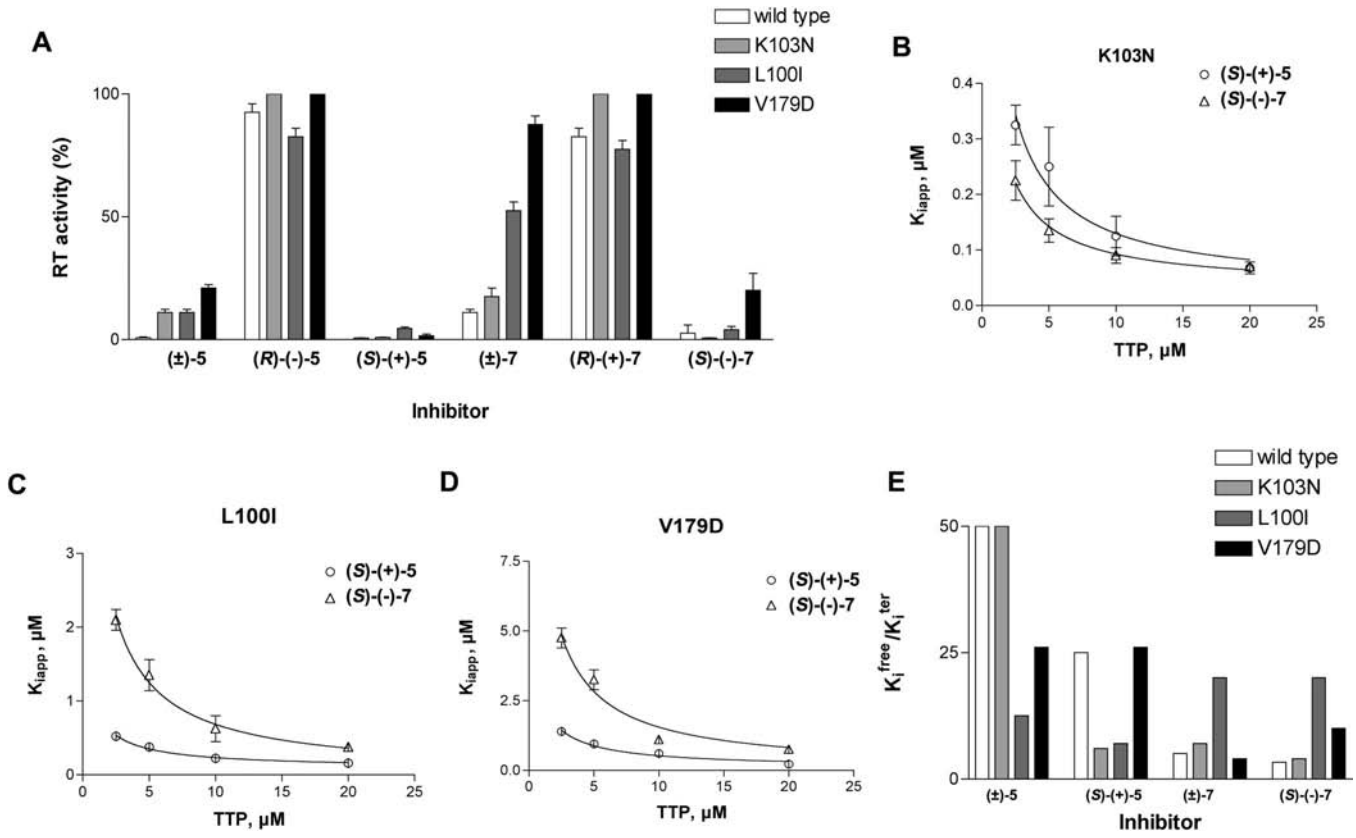

Figure 1. (A) Residual activity of HIV-1 RT tested with PBOs and PPOs (10 μM). RTwt is represented in white bars, K103N in light gray bars, L100I in dark gray bars, and V179D in black. (B−D) Decrease of K_{iapp} (μM) of (*S*)-(+)-**5** (circles) and (*S*)-(−)-**7** (triangles) vs K103N (B), L100I (C), and V179D (D). HIV-1 RT was tested on poly (rA)/oligo dT in presence of the different derivatives under the conditions described in the Supporting Information in the presence of different fixed concentrations of TTP (1.5, 2.5, 10, and 20 μM). The K_{iapp} for different inhibitors at each substrate concentrations were calculated from eq 1 as described in the Supporting Information. The variation of the K_{iapp} values as a function of the TTP concentrations was analyzed according to eq 2 (in the Supporting Information) to calculate the true K_i^{ter} values. (E) Variation of K_i values for the ternary complex. Each inhibitor was tested vs RTwt (white), K103N (light gray), and V179D (black).

of inhibitors typified by the pyrrolopyridooxazepinone (PPO) **3b** (Chart 1). These analogues were potent antiviral agents selectively targeting the HIV-1 RT ternary complex, and potentially useful in combination with NNRTIs selectively binding the free enzyme or the binary complex.[8] Recently, we further improved the pharmacological profile of PBOs by synthesizing a series of C6-modified derivatives of **3a** capable of specifically targeting the highly conserved amino acid residues within the $\beta12-\beta13$ hairpin (F227, W229, M230). The resulting C6-extended analogues (typified by **4**, Chart 1) were identified as novel NNRTIs characterized by high antiviral efficacy and improved mutant resilience.[9] Herein we describe the chemical and biological characterization of PBOs and novel PPOs. Antiviral activity and drug resistance profiles of racemates ((±)-**5**,[9] (±)-**6**, and (±)-**7**, Chart 1) are compared to those of the pure enantiomers ((*S*)-(+)-**5**, (*R*)-(−)-**5**, (*S*)-(−)-**7**, and (*R*)-(+)-**7**) vs RT wild type and its mutant forms (K103N, L100I, V179D, Tables 1−2, Table 1 of the Supporting Information (SI), and Figures 1−3). A stereoselective interaction of the pure enantiomers with the HIV-1 RT, which also correlates with cellular assays, was demonstrated and rationalized through a molecular modeling study.

Biological Results and Discussion

In enzymatic assays, compounds (±)-5-**7** demonstrated good inhibitory properties against RT wild type and its mutant forms (L100I, K103N, Y181I, V106A, V179D, and Y188L, Table 1). In general, compounds (±)-**5** and (±)-**7** were more potent than (±)-**6**. Therefore they were selected for further biological studies, their enantiomers were separated by HPLC techniques, and the absolute configuration was determined by X-ray analysis (Figure 1 SI and Figure 2 SI).

When the residual activity of wild type and mutant forms of HIV-1 RT was tested in the presence of (±)-**5**, (±)-**7**, and their

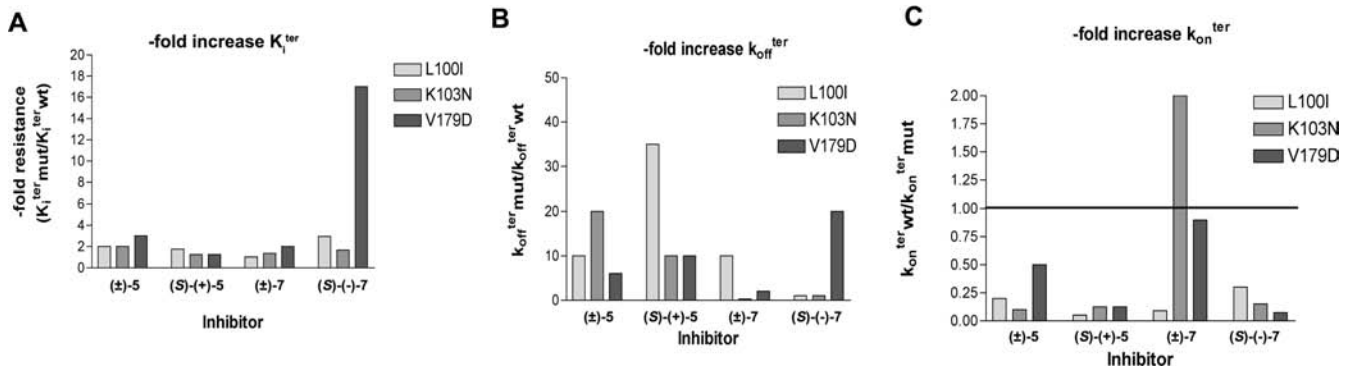

Figure 2. (A) Values of fold resistance derived from the ratio K_i^{ter}mutant/K_i^{ter}wt. (B) Values of the k_{off}^{ter}mutant/k_{off}^{ter}wt representing the fold increase in rate of dissociation. (C) Values of the k_{on}^{ter}wt/k_{on}^{ter}mutant representing the fold decrease in rate of association.

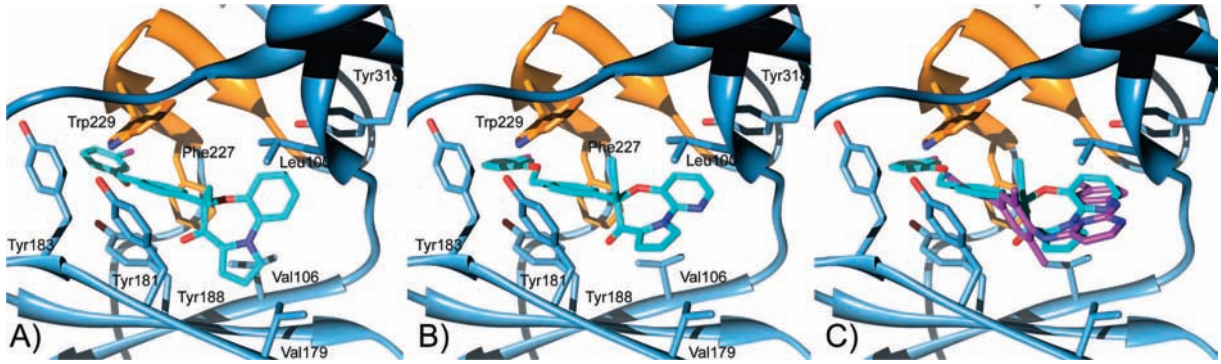

Figure 3. Docked structures of (*S*)-(+)-**5** (A), and (*S*)-(−)-**7** (B), (*S*)-(−)-**7** in comparison with the experimentally found structure of TMC278 (C) in the 3D crystal structure of HIV-1 RT (PDB code 2ZD1). Hydrogens are omitted for sake of clarity. (*S*)-(+)-**5** and (*S*)-(−)-**7** are displayed with white sticks, TMC278 is displayed with magenta sticks, and key interacting residues are shown in blue or orange if belonging to the primer grip region. The figure was created using Chimera software.[11]

Table 2. Inhibition of HIV-IIIB Replication and Cytotoxicity in C8166 Cells

	cell. assays[a]		
compd	EC_{50} (μM)[b]	TC_{50} (μM)[c]	TI_{50}[d]
(±)−**5**	0.1500	40.300	268.66
(*R*)−(−)−**5**	4.7000	60.880	12.950
(*S*)−(+)−**5**	0.0440	106.21	2413.0
(±)−**7**	0.0690	12.600	182.60
(*R*)−(+)−**7**	1.9400	0.0188	<103.19
(*S*)−(−)−**7**	0.0500	111.39	<2227.2
8-ClTIBO	0.0300	50.10	1670.0
AZT	0.0019	<1	<526.32
efavirenz	0.0027	<1	<370.37

[a] All the data listed were compared to the corresponding test results for AZT, which served as the treated control, and 8-ClTIBO performed at the same time. [b] The EC_{50} value is the test drug concentration that produces a 50% survival of HIV-1 infected cells relative to uninfected untreated controls (e.g., in vitro anti-HIV-1 activity). [c] TC_{50} value is the test drug concentration that results in a 50% death of uninfected untreated control C8166 cells (e.g., cytotoxicity of the test drug). [d] TI_{50} therapeutic index (TC_{50}/EC_{50}).

(*R*)- and (*S*)- enantiomers (Figure 1A), (*S*)-(+)-**5**, (*S*)-(−)-**7**, and (±)-**5** significantly inhibited HIV-1 RT, both in its wild type and mutant forms, whereas the enantiomers (*R*)-(−)-**5** and (*R*)-(+)-**7** were almost inactive. These results indicate a strictly stereoselective mode of inhibition. (*S*)-(+)-**5** and (*S*)-(−)-**7** showed an increase in potency (reduction of the apparent inhibition constants K_{iapp} values), which was dependent on the thymidine triphosphate (TTP) concentrations (Figure 1B−D). From these data, it was possible to calculate the true dissociation constant (K_i^{ter}) for binding of each inhibitor to the ternary complex between the enzyme and its substrates nucleic acid and dNTP. The derived values are listed in Table 1 SI. For all the inhibitors tested, the apparent binding constant for the free enzyme (K_i^{free}) values were almost equal to those for the binary complex [E:DNA] (K_i^{bin}), whereas the K_i^{ter} values were significantly lower. These data clearly indicate a higher affinity of (*S*)-(+)-**5** and (*S*)-(−)-**7** for the catalytically competent ternary complex of HIV-1 RT. In particular, we calculated the K_i^{free}/K_i^{ter} (Table 1 SI and Figure 1E) in order to estimate the magnitude of the decrease of K_i values for the ternary complex with respect to the free enzyme for the mutant forms. It resulted that (±)-**5** showed the highest selectivity toward the K103N ($K_i^{free}/K_i^{ter} = 50.0$) enzyme, whereas (±)-**7** and (*S*)-(−)-**7** showed the highest selectivity for the L100I mutant ($K_i^{free}/K_i^{ter} = 20.0$). The selectivity of (±)-**5** for V179D ($K_i^{free}/K_i^{ter} = 23.3$) was similar to (*S*)-(+)-**5** ($K_i^{free}/K_i^{ter} = 26.0$). We also compared the K_i^{ter} mutant/K_i^{ter} wt for (±)-**5**, (±)-**7**, (*S*)-(+)-**5**, and (*S*)-(−)-**7** (Figure 2A, in the form of bar plots) to determine the relative-fold resistance. When compared to the wild type RT, all the compounds showed very low resistance values (K_i^{ter}mutant/K_i^{ter}wt ≤ 3) with the exception of V179D mutant toward (*S*)-(−)-**7** (-fold resistance values of 16.7). An inhibitor could show a lower affinity for its target enzyme by either a decreased association rate (k_{on}), or an increased dissociation rate (k_{off}), or both. To elucidate the mechanism responsible for the observed resistance toward our compounds, equilibrium binding experiments were performed (as described in Supporting Information) with the aim of determining the association (k_{on}) and dissociation (k_{off}) rates for all the inhibitors to the different RT forms (free enzyme, binary complex, and the catalytically competent ternary complex) along the enzyme's reaction pathway, with HIV-1 RT wild type and L100I, K103N, and V179D mutants. The calculated k_{on} and k_{off} values (Table 1 SI) for the binary and ternary complexes were then compared to each other and to

the corresponding values for the free enzyme. The values of k_{off}^{ter} mutant/k_{off}^{ter}wt, indicating the -fold increase in the dissociation constant (k_{off}), are shown in Figure 2B. The values of the k_{on}^{ter}wt/k_{on}^{ter} mutant, measuring the -fold decrease in the association constant (k_{on}) for the different RT mutants, are shown in Figure 2C. As can be seen, (±)-**7** and (*S*)-(−)-**7** showed no significant variations in their k_{off} rates in the case of the mutant K103N, whereas the L100I and V179D mutations caused an increase in the k_{off} rates of either (±)-**7** or (*S*)-(−)-**7**, respectively. Compounds (±)-**5** and (*S*)-(+)-**5** showed an increase in their dissociation rates for all the mutants tested (Figure 2B). Remarkably, all the compounds (with the only exception of (±)-**7** toward K103N) showed increased association rates to the mutants with respect to the wild type RT (Figure 2C), as indicated by the -fold increase in k_{on} values <1. Thus, the relatively low level of resistance of these inhibitors (Figure 2A) can be explained by faster dissociation rates from the mutants (Figure 2B), which are in turn compensated by higher association rates (Figure 2C).

Cellular tests were performed in order to evaluate ability of inhibiting syncytia formation on C8166 cells infected with wild-type HIV-1IIIB virus (Table 2). These tests were in line with enzymatic assays, and confirmed better activity of the *S* enantiomers. (*S*)-(+)-**5** and (*S*)-(−)-**7** showed a very potent antiviral efficacy in C8166 cells, similar to that of 8-ClTIBO. They also exhibited extremely favorable therapeutic indexes, being endowed with low toxicity for C8166 noninfected cells (TC_{50} between 106.2 and 11.4 μM).

Molecular Modeling Studies

The binding interactions established by our PBOs with wild type HIV-1 RT were probed in previous studies[6] and led to the rational design of new derivatives (typified by **4**), characterized by an extended substitution at the C6-pendant phenyl ring.[9b] Such a modification allowed a specific targeting of highly conserved residues (e. g., W229), thus resulting in a lower sensitivity to resistance mutations. In the same studies, the (*S*)-enantiomer of these compounds was predicted to be the active one.[9b] Moreover, the isosteric switch from the PBO scaffold to the PPO tricyclic system resulted in new derivatives still endowed with inhibitory activity against HIV-1 RT and some of its mutants.[8]

Herein, we confirm our previous assumptions for the C6-extended PBO analogue **5** by resolving the racemate into the pure enantiomers, and we present two new PPO C6-extended analogues, **6** and **7**, of which only the (*S*)-enantiomer was demonstrated to be active. In the present study, the reasons for the stereoselective binding of **5** and **7** in the HIV-1 RT allosteric binding site were investigated using a well-known ligand−receptor docking approach (Autodock program (vs 4.0)). The three-dimensional (3D) structure of wild type HIV-1 RT has been reported in complex with several inhibitors and, so far, more than 50 structures have been deposited on the Protein Data Bank (PDB). To take into account the intrinsic plasticity displayed by RT in the interaction with different NNRTIs, we decided to use the nine highest resolution X-ray complexes (see Supporting Information for details) to dock both the pseudoaxial and pseudoequatorial pendant phenyl ring conformations of the aforementioned ligands. A first analysis of the docking results was made by taking into account the binding free energies (ΔG_{AD4}) associated to the best (lowest energy) predicted ligand−enzyme complexes for the nine X-ray structures (Table 2 SI). Then the lowest energy conformations of each calculated ligand−enzyme complex was visually inspected and related to experimental data (SARs and site-directed mutagenesis). In our previous paper,[9a] SAR analysis demonstrated that the PBO scaffold itself and the pendant phenyl at the C6 position are both involved in the interaction with the enzyme. Moreover, the elongation of the pendant branch with a phenyloxymethyl moiety was demonstrated to be crucial for activity. On the basis of these experimental data, we discarded all the solutions in which either the PBO scaffold or the pendant moiety at C6 did not take direct contact with the enzyme binding site. In regards to the (*S*)-enantiomers, this criterion allowed retention of only the solutions calculated for the pseudoequatorial (*S*)-(+)-**5**, and (*S*)-(−)-**7** in complex with RT structure coded 2ZD1.[10] This latter is the enzyme conformation in which the inspected ligands can better accommodate themselves. Accordingly, docking on this 3D binding site structure produced the lowest ΔG_{AD4} values (see Table 2 SI) with respect to the other docking experiments. A close analysis of the computational results for the pseudoequatorial (*S*)-(+)-**5** revealed a binding motif with the benzo-fused ring of (*S*)-(+)-**5** in proximity of the L100 side chain, engaged in a T-shaped interaction with Y318, while the pyrrole ring establishes favorable van der Waals contacts with V179 and V106 (Figure 3A). Consequently, the ethyl at C6 was in close contact with L100, while the pendant phenyl ring was embedded in the aromatic cleft delimited by Y181, Y188, F227, and W229 residues establishing multiple charge-transfer interactions. This region is flanked on one side by the $\beta9-\beta10$ hairpin and on the other by the so-called primer grip region ($\beta12-\beta13$ hairpin), which is known to be directly involved in the catalytic polymerase activity of HIV-1 RT.[9a] The phenyloxymethyl branch is in close proximity with the primer grip region and engages a T-shaped interaction with Y183 side chain, which is reinforced by the electron-withdrawing *meta*-chlorine atom. This latter residue was demonstrated to be crucial for the enzyme polymerase activity being part of the YMDD motif in the $\beta9-\beta10$ hairpin.[10] In regard to the C6-extended PPO analogue **7**, the enantiomers were separated and (*S*)-(−)-**7** was found as the active enantiomer. Docking studies highlighted binding interactions for (*S*)-(−)-**7** similar to (*S*)-(+)-**5** (Figure 3B). Interestingly, when comparing the predicted poses for both (*S*)-(+)-**5** and (*S*)-(−)-**7** with the experimental one found for TMC278 cocrystallized with HIV-1 RT in 2ZD1, an impressive resemblance was found despite the chemical diversity (Figure 3C). It is worth noting that the above-described binding poses were not detected in the other used X-ray structures due to a different conformation of the $\beta9-\beta10$ hairpin that occludes the aromatic tunnel formed by the primer grip and the hairpin itself (see Figure 3 SI). If compared with the results obtained for the (*S*)-enantiomers, a diverse behavior was observed for the (*R*)-ones. In fact, regardless the enzyme conformation, the phenyloxymethyl branch did not allocate itself in the NNRTIs binding site and is rather solvent exposed. Moreover, in the 2ZD1 conformation, the lowest energy pose of both (*R*)-(−)-**5** and (*R*)-(+)-**7** does not allow any interaction with the residues in both the primer grip region and the $\beta12-\beta13$ hairpin (Figure 4 of Supporting Information). Visual inspection of the crystal structure of HIV-1 RT in complex with AZTMP-terminated DNA reveals that the aforementioned primer grip region is placed underneath the DNA. However, this portion in the predicted (*S*)-PBO/enzyme and (*S*)-PPO/enzyme complexes sterically hampers the interaction with the DNA (Figure 5 SI). Therefore, it is likely that (*S*)-(+)-**5** and (*S*)-(−)-**7** exert their inhibitory activity against HIV-1 RT by stabilizing a specific conformation of the primer grip region and by preventing its

relocation. Consequently, the inactivity of the (*R*)-isomers may be due to the lack of interaction with the primer grip region of RT.

Conclusions

We identified (*S*)-(+)-**5** and (*S*)-(−)-**7** as stereoselective inhibitors of HIV-1 RT, and specific drug resistance RT mutations (K103N, L100I and V179D) were demonstrated to differentially affect enzyme sensitivity to the active compounds and their racemic forms. Moreover, a selective binding for the catalytically competent ternary complex of HIV-1 RT was also demonstrated for these ligands. Cellular assays substantially confirmed activity of the compounds and are in line with stereoselectivity of interaction with HIV-1 RT. Molecular modeling studies provided an explanation of this behavior at the molecular level.

Experimental Procedures

The synthesis of compounds (±)-**6** and (±)-**7** was performed according to Scheme 1 as reported in SI. We describe herein the synthesis of the final compounds (±)-**6** and (±)-**7**.

(±)-6-Ethyl-6-[4-(phenyloxymethyl)phenyl]-6,7-dihydropyrrolo[1,2-*d*]pyrido[3,2-*b*][1,4]oxazepin-7-one ((±)-6). To a solution of phenol (22 mg, 0.23 mmol) in dry tetrahydrofuran (2.0 mL), sodium *tert*-butoxide (30 mg, 0.31 mmol) was added, and the resulting mixture was heated to 40 °C. After 1 h, a solution of bromide **9** (60 mg, 0.15 mmol) in dry terahydrofuran (2.0 mL) was slowly added, and the resulting mixture was stirred overnight. The solvent was removed in vacuo, and the residue was taken up with dichloromethane. The organic phase was washed with brine, dried, and concentrated. The residue was purified by means of flash chromatography (dichloromethane/methanol 19:1) to give (±)-**6** as a white amorphous solid (73% yield): ^{1}H NMR ($CDCl_3$) δ 1.08 (t, 3H, J = 7.4 Hz), 2.42 (q, 2H, J = 7.5 Hz), 4.92 (s, 2H), 6.47 (m, 1H), 6.75−6.79 (m, 1H), 6.89−6.96 (m, 2H), 7.00−7.05 (m, 1H), 7.13−7.42 (m, 8H), 7.49 (m, 1H), 8.08 (m, 1H). Anal. ($C_{26}H_{22}N_2O_3$) C, H, N.

(±)-6-Ethyl-6-[4-[(3-chlorophenyloxy)methyl]phenyl]-6,7-dihydropyrrolo[1,2-*d*]pyrido[3,2-*b*][1,4]oxazepin-7-one ((±)-7). (±)-**7** was obtained following the procedure described for (±)-**6**. The residue was purified by flash chromatography (dichloromethane/methanol 19:1) to give (±)-**7** as a white amorphous solid (69% yield): ^{1}H NMR ($CDCl_3$) δ 1.09 (t, 3H, J = 7.5 Hz), 2.43 (m, 2H), 4.93 (s, 2H), 6.48 (m, 1H), 6.75−6.79 (m, 1H), 6.89−6.94 (m, 2H), 7.00−7.05 (m, 1H), 7.13−7.39 (m, 7H), 7.49 (m, 1H), 8.09 (m, 1H); ^{13}C NMR (75 MHz, $CDCl_3$) δ 8.9, 33.7, 69.7, 94.4, 112.0, 113.5 115.5, 121.5, 122.3, 123.4, 126.8, 127.3, 128.1, 130.5, 132.9, 134.3, 135.1, 136.9, 137.5, 141.9, 143.9, 144.7, 159.5, 189.4; ESI-MS *m*/*z* 445 $(M + H)^+$, 466 (100) $(M + Na)^+$. Anal. ($C_{26}H_{21}ClN_2O_3$) C, H, N.

Acknowledgment. We thank the European Research Centre for Drug Discovery and Development for financial support. S.Z. is the recipient of a Buzzati-Traverso Fellowship.

Supporting Information Available: Elemental analyses for final compounds, Table for enzymatic assays, chemistry, experimental procedures for intermediates, HPLC separation of (±)-**5** and (±)-**7**, enantiomers crystallization, X-ray crystallography, biological assays, and molecular modeling. This material is available free of charge via the Internet at http://pubs.acs.org.

References

(1) De Clercq, E. HIV Inhibitors targeted at the reverse transcriptase. *AIDS Res. Hum. Retrovirus* **1992**, *8*, 119–134.
(2) Kauffmann, G. R.; Cooper, D. A. Antiretroviral therapy of HIV-1 infection: Established treatment strategies and new therapeutic options. *Curr. Opin. Microbiol.* **2000**, *3*, 508–514.
(3) Tomassi, C.; Van Nhien, A. N.; Marco-Contelles, J.; Balzarini, J.; Pannecouque, C.; De Clercq, E.; Soriano, E.; Postela, D. Synthesis, anti-HIV-1 activity, and modeling studies of N-3 Boc TSAO compound. *Bioorg. Med. Chem. Lett.* **2008**, *18*, 2277–2281.
(4) Campiani, G.; Ramunno, A.; Maga, G.; Nacci, V.; Fattorusso, C.; Catalanotti, B.; Morelli, E.; Novellino, E. Non-nucleoside HIV-1 reverse transcriptase (RT) inhibitors: past, present, and future perspectives. *Curr. Pharm. Des.* **2002**, *8*, 615–657.
(5) Maga, G.; Ubiali, D.; Salvetti, R.; Pregnolato, M.; Spadari, S. Selective interaction of the human immunodeficiency virus type 1 reverse transcriptase nonnucleoside inhibitor efavirenz and its thio-substituted analog with different enzyme−substrate complexes. *Antimicrob. Agents Chemother.* **2000**, *44*, 1186–1194.
(6) Campiani, G.; Morelli, E.; Fabbrini, M.; Nacci, V.; Greco, G.; Novellino, E.; Ramunno, A.; Maga, G.; Spadari, S.; Caliendo, G.; Bergamini, A.; Faggioli, E.; Uccella, I.; Bolacchi, F.; Marini, S.; Coletta, M.; Nacci, A.; Caccia, S. Pyrrolobenzoxazepinone derivatives as non-nucleoside HIV-1 RT inhibitors: Further structure−activity relationship studies and identification of more potent broad-spectrum HIV-1 RT inhibitors with antiviral activity. *J. Med. Chem.* **1999**, *42*, 4462–4470.
(7) Locatelli, G. A.; Campiani, G.; Cancio, R.; Morelli, E.; Ramunno, A.; Gemma, S.; Hubscher, U.; Spadari, S.; Maga, G. Effects of drug resistance mutations L100I and V106A on the binding of pyrrolobenzoxazepinone nonnucleoside inhibitors to the human immunodeficiency virus type 1 reverse transcriptase catalytic complex. *Antimicrob. Agents Chemother.* **2004**, *48*, 1570–1580.
(8) Maga, G.; Ramunno, A.; Nacci, V.; Locatelli, G. A.; Spadari, S.; Fiorini, I.; Baldanti, F.; Paolucci, S.; Zavatoni, M.; Bergamini, A.; Galletti, B.; Muck, S.; Hubscher, U.; Giorgi, G.; Guiso, G.; Caccia, S.; Campiani, G. The stereoselective targeting of a specific enzyme-substrate complex is the molecular mechanism for the synergic inhibition of HIV-1 reverse transcriptase by (*R*)-(−)-PPO464. *J. Biol. Chem.* **2001**, *276*, 44653–44662.
(9) (a) Fattorusso, C.; Gemma, S.; Butini, S.; Huleatt, P.; Catalanotti, B.; Persico, M.; De Angelis, M.; Fiorini, I.; Nacci, V.; Ramunno, A.; Rodriguez, M.; Greco, G.; Novellino, E.; Bergamini, A.; Marini, S.; Coletta, M.; Maga, G.; Spadari, S.; Campiani, G. Specific targeting highly conserved residues in the HIV-1 reverse transcriptase primer grip region. Design, synthesis, and biological evaluation of novel, potent, and broad spectrum NNRTIs with antiviral activity. *J. Med. Chem.* **2005**, *48*, 7153–7165. (b) Zanoli, S.; Gemma, S.; Butini, S.; Brindisi, M.; Joshi, B. P.; Campiani, G.; Fattorusso, C.; Persico, M.; Crespan, E.; Cancio, R.; Spadari, S.; Hübscher, U.; Maga, G. Selective targeting of the HIV-1 reverse transcriptase catalytic complex through interaction with the "primer grip" region by pyrrolobenzoxazepinone non-nucleoside inhibitors correlates with increased selectivity towards drug-resistant mutants. *Biochem. Pharmacol.* **2008**, *76*, 156–168.
(10) Das, K.; Bauman, J. D.; Clark, A. D., Jr.; Frenkel, Y. V.; Lewi, P. J.; Shatkin, A. J.; Hughes, S. H.; Arnold, E. High-resolution structures of HIV-1 reverse transcriptase/TMC278 complexes: Strategic flexibility explains potency against resistance mutations. *Proc. Natl. Acad. Sci. U.S.A.* **2008**, *105*, 1466–1471.
(11) Pettersen, E. F.; Goddard, T. D.; Huang, C. C.; Couch, G. S.; Greenblatt, D. M.; Meng, E. C.; Ferrin, T. E. UCSF Chimera−A Visualization system for exploratory research and analysis. *J. Comput. Chem.* **2004**, *25*, 1605–1612.

JM801395V